NIH Public Access
Author Manuscript
Cell. Author manuscript; available in PMC 2013 October 12.

Published in final edited form as:
Cell. 2012 October 12; 151(2): 372–383. doi:10.1016/j.cell.2012.08.036.

TPC Proteins Are Phosphoinositide-activated Sodium-selective Ion Channels in Endosomes and Lysosomes

Xiang Wang[1,#], **Xiaoli Zhang**[1,#], **Xian-ping Dong**[1], **Mohammad Samie**[1], **Xinran Li**[1], **Xiping Cheng**[1], **Andrew Goschka**[1], **Dongbiao Shen**[1], **Yandong Zhou**[2], **Janice Harlow**[2], **Michael X. Zhu**[3], **David E. Clapham**[4], **Dejian Ren**[2], and **Haoxing Xu**[1,*]

[1]Department of Molecular, Cellular, and Developmental Biology, the University of Michigan, 3089 Natural Science Building (Kraus), 830 North University, Ann Arbor, MI 48109, USA

[2]Department of Biology, University of Pennsylvania, Philadelphia, PA 19104, USA

[3]Department of Integrative Biology & Pharmacology, University of Texas Health Science Center at Houston, Houston, TX 77030, USA

[4]Department of Cardiology, Children's Hospital Boston, Enders 1350, 320 Longwood Avenue, Boston, MA 02115, USA

Summary

Mammalian Two-Pore Channels (TPC1, 2; *TPCN1, TPCN2*) encode ion channels in intracellular endosomes and lysosomes and were proposed to mediate endolysosomal calcium release triggered by the second messenger, nicotinic acid adenine dinucleotide phosphate (NAADP). By directly recording TPCs in endolysosomes from wild-type and TPC double knockout mice, here we show that, in contrast to previous conclusions, TPCs are in fact sodium-selective channels activated by $PI(3,5)P_2$, and are not activated by NAADP. Moreover, the primary endolysosomal ion is Na^+, not K^+, as had been previously assumed. These findings suggest that the organellar membrane potential may undergo large regulatory changes, and may explain the specificity of $PI(3,5)P_2$ in regulating the fusogenic potential of intracellular organelles.

Keywords

Whole-endolysosome patch-clamp; Two-pore channel (TPC); PIKfyve; phosphoinositide; $PI(3,5)P_2$; Na^+ channel; lysosome; membrane trafficking

© 2012 Elsevier Inc. All rights reserved.

*To whom correspondence should be addressed: haoxingx@umich.edu.
#These authors contributed equally to this work.

Author contribution: the authors were listed in the order of their institutions; X.W. initiated the project; X.W., X.Z, and X.D. performed the electrophysiology experiments; X.W also performed the Ca^{2+} imaging experiments; M.S. and A. G. performed the ionic composition experiments; X. L., X. C., D.S., and M.X.Z contributed the reagents; D.R. and J.H. developed the *TPC1, TPC2* knockout mouse lines, the *hTPC1, hTPC2, hTPC1ΔN* and *hTPC2ΔN* constructs; Y.Z. measured the glucose- and NAADP -induced Ca^{2+} responses in the TPC mutant islets compared with wild-type; development of TPC1 knockout was carried out by D.R. in the laboratory of D.E.C; H.X. and D.E.C. wrote the paper with input from all authors. We are grateful to Drs. Susan Slaugenhaupt and James Slama for sharing the reagents, Drs. Ted Huston, Hollis Showalter, Yafei Jin, Leslie Satin, Jianhua Ren, Peter Arvan, and Dr. Gautam Rajpal for assistance, and Dr. Richard Hume for comments on an earlier version of the manuscript. We appreciate the encouragement and helpful comments from other members of the Xu, Ren, and Clapham laboratories.

Publisher's Disclaimer: This is a PDF file of an unedited manuscript that has been accepted for publication. As a service to our customers we are providing this early version of the manuscript. The manuscript will undergo copyediting, typesetting, and review of the resulting proof before it is published in its final citable form. Please note that during the production process errors may be discovered which could affect the content, and all legal disclaimers that apply to the journal pertain.

NIH-PA Author Manuscript
NIH-PA Author Manuscript
NIH-PA Author Manuscript

NIH-PA Author Manuscript
NIH-PA Author Manuscript
NIH-PA Author Manuscript

Introduction

Two-pore channel proteins (TPC1, 2; *TPCN1, TPCN2*) (Calcraft et al., 2009; Morgan et al., 2011) are localized in the intracellular endosomes and lysosomes (collectively endolysosomes) previously inaccessible to conventional patch clamp assays. Consistent with this localization, human genetic studies have identified TPC2 as a regulator of pigmentation (Sulem et al., 2008), and a number of recent studies suggest that TPCs mediate Ca^{2+} release from endolysosomes in response to an elevation of the potent Ca^{2+}-mobilizing second messenger, nicotinic acid adenine dinucleotide phosphate (NAADP) (Brailoiu et al., 2009; Calcraft et al., 2009; Ruas et al., 2010; Zong et al., 2009) (but also see ref. (Guse, 2009)). Unlike plasma membrane-localized Na_V and Ca_V channels, the primary structures of TPCs contain two, instead of four, 6 transmembrane (6TM) domains (Yu and Catterall, 2004). Like Na_V and Ca_V channels, they contain multiple positively charged amino acid residues in their voltage sensor domains, and negatively-charged amino acid residues in their pore domains, but their intracellular localization has prevented characterization of basic channel properties such as selectivity and gating.

$PI(3,5)P_2$ is an endolysosome-specific phosphoinositide (PIP) of low abundance (Dove et al., 2009; Shen et al., 2011). Upon cellular stimulation PIKfyve/Fab1, PI 5-kinase phosphorylates PI(3)P to increase $PI(3,5)P_2$ from low nM to μM concentrations (Dove et al., 2009; Shen et al., 2011). Human mutations in $PI(3,5)P_2$-metabolizing enzymes and their regulators result in muscle and neurodegenerative diseases such as amyotrophic lateral sclerosis (ALS) and Charcot-Marie-Tooth (CMT-4B, CMT-4J) disease (Chow et al., 2007). $PI(3,5)P_2$-deficient cells have enlarged endolysosomes/vacuoles, suggestive of impaired ion homeostasis and/or defective membrane trafficking (Chow et al., 2007; Dove et al., 2009; Kerr et al., 2010; Shen et al., 2011). We recently found that TRPML1 mediates $PI(3,5)P_2$-dependent Ca^{2+} release from endolysosomes (Dong et al., 2010a). However, $PI(3,5)P_2$ deficiency results in a much more severe phenotype than TRPML1 mutations, suggesting that there are additional $PI(3,5)P_2$ effectors (Shen et al., 2011). Here, we find by direct patch-clamp of endolysosomal membranes, that $PI(3,5)P_2$ specifically activates TPCs, and unexpectedly, that NAADP does not. TPC-mediated currents are selective for Na^+, which we demonstrate is the predominant cation in the lysosome. TPCs represent the first intracellular Na^+-selective channels, and suggest a new model for ion channel control of endolysosomal fusion.

Results

$PI(3,5)P_2$ activation of a large endogenous current in the endolysosome

Cells were pretreated with vacuolin-1, a lipid-soluble polycyclic triazine (Huynh and Andrews, 2005) that can selectively increase the size of endosomes and lysosomes from < 0.5 μm to up to 5 μm (Dong et al., 2010a). The enlarged endolysosomes were manually isolated and then patch clamped in the whole-endolysosome configuration (Fig. 1A; see Suppl. fig. S1). We previously reported that TRPML1 was the primary $PI(3,5)P_2$-activated conductance (reversal potential, $E_{rev} \sim 0$ mV) in the endolysosomes of human fibroblasts (Dong et al., 2010a). However, in several other cell types including skeletal muscles (data not shown) and macrophages, we observed that bath (cytoplasmic) application of diC8 $PI(3,5)P_2$ (abbreviated as $PI(3,5)P_2$), a water-soluble analog of $PI(3,5)P_2$ (Dong et al., 2010a), activated a distinct whole-endolysosome conductance with an $E_{rev} > +60$ mV (defined as I_X; Fig. 1B). Strongly inwardly-rectifying TRPML-like currents ($I_{TRPML\text{-}L}$; (Dong et al., 2010a)) were also present in macrophages, but $PI(3,5)P_2$-activated $I_{TRPML\text{-}L}$ was often masked by I_X due to its positive E_{rev}. $I_{TRPML\text{-}L}$ could be activated by SF-51 (100 μM (Grimm et al., 2010); Fig. 1B). $I_{TRPML\text{-}L}$, but not I_X, was dramatically reduced in *TRPML1*$^{-/-}$ macrophages (Fig. 1C). In 9 out of 23 enlarged endolysosomes isolated from

NIH-PA Author Manuscript

NIH-PA Author Manuscript

NIH-PA Author Manuscript

non-transfected COS-1 cells, high concentrations of $PI(3,5)P_2$ (10 μM) activated I_X, which was distinct from $I_{TRPML\text{-}L}$ activated by 1 μM $PI(3,5)P_2$ (Dong et al., 2010a) or SF-51 (Fig. 1D).

$PI(3,5)P_2$ activates recombinant TPC1 and TPC2 channels in the endolysosome

To search for the identity of the protein mediating I_X, a number of fluorescently-tagged putative intracellular channels or transporter-like lysosomal membrane proteins were transfected into COS-1 cells. As described below, endolysosomes from TPC1- and TPC2-transfected cells exhibit large *I*x. The majority (> 80%) of vacuolin-1-treated TPC2-positive vacuoles were Lamp-1^+ (Fig. 2A), confirming that TPC2-positive vacuoles were enlarged late endosomes and lysosomes (LELs). In TPC2 (hTPC2)-positive enlarged LELs isolated from transfected COS1 cells, little or no basal currents were detected in the whole-endolysosome configuration (Fig. 2B). Bath application of $PI(3,5)P_2$ rapidly activated hTPC2-mediated currents (I_{TPC2}; E_{rev} = + 83 ± 3 mV; Fig. 2B), but not those that expressed a mutant hTPC2 carrying a charge-reversal mutation in the putative pore domains (D276K; see Suppl. fig. S2A, B); I_{TPC2} gradually declined upon the washout of $PI(3,5)P_2$ (Fig. 2B) with variable time courses (depending on treatment time). The I-V and E_{rev} of I_{TPC2} are similar to the endogenous $PI(3,5)P_2$-activated I_X.

$PI(3,5)P_2$-dependent activation of I_{TPC2} was dose-dependent (EC_{50}= 390 ± 94 nM; Fig. 2C). I_{hTPC2} was inhibited > 80% by the $PI(3,5)P_2$ chelators (Nilius et al., 2008; Suh and Hille, 2008) poly-L-lysine and anti-$PI(3,5)P_2$ antibody (Suppl. fig. S2C, D). Other phosphoinositides, PI(3)P, PI(5)P, $PI(3,4)P_2$, $PI(4,5)P_2$, and $PI(3,4,5)P_3$, did not activate I_{TPC2} (10 μM; Fig. 2D Suppl. fig. S2E). Thus $PI(3,5)P_2$ activated I_{TPC2} with striking specificity. In contrast, 1 μM $PI(3,5)P_2$ failed to activate the lysosome-localized (Lange et al., 2009) recombinant TRPM2 channel (Suppl. fig. S2F) or modulate the endogenous outward currents that were present in a subset of endolysosomes isolated from INS1 pancreatic β-cells (Suppl. fig. S2G). TPC1, also localized in the endolysosome (Calcraft et al., 2009) (but primarily in Lamp-1-negative compartments; Suppl. fig. S2A), was also activated by $PI(3,5)P_2$ (Fig. 2E).

TPC-mediated currents are Na^+-selective

The measured E_{rev} of I_{TPC} under standard recording conditions (with a low pH modified Tyrode's solution in the pipette/lumen and a K^+-based solution in the bath/cytosol) dictates that the channels are selective for Na^+, Ca^{2+}, or H^+, but not K^+. Increasing the luminal pH from 4.6 to 7.4 had minimal effects on I_{TPC2} (Fig. 3A; Suppl. fig. S3A) and I_{TPC1}. Conversely, replacement of luminal cations (Na^+, K^+, Mg^{2+}, and Ca^{2+}) with $NMDG^+$ at pH 4.6 completely abolished inward I_{TPC2} (Suppl. fig. S3B), suggesting that I_{TPC2} is impermeable to H^+ or $NMDG^+$. Under bi-ionic conditions (luminal Na^+, pH 7.4; cytoplasmic K^+), the E_{rev} of I_{TPC2} was + 89 ± 5 mV (n=8; see Fig. 3A). In contrast, under reversed bi-ionic conditions (luminal K^+, pH 7.4; cytoplasmic Na^+), the E_{rev} of I_{TPC2} was −68 ± 3 mV (n = 5; see Fig. 3B). These results indicated that I_{TPC2} was selective for Na^+ over K^+. Consistent with this conclusion, switching cytoplasmic K^+ to Na^+ in the presence of luminal Na^+ resulted in a leftward shift of the E_{rev} and the appearance of large outward currents (Fig. 3A). Addition of 2 mM Ca^{2+} to the luminal side of the symmetric Na^+ solutions did not result in any significant change of the E_{rev} or the amplitude of the inward currents (see Suppl. fig. S3C), suggesting that luminal Ca^{2+} contributed insignificantly to inward I_{TPC2}. Consistently, under bi-ionic conditions (luminal isotonic Ca^{2+}, pH 4.6 or 7.4; cytoplasmic Na^+), the E_{rev} of I_{TPC2} was −68 ± 2 mV (n = 12; see Suppl. fig. S3D), in dramatic contrast to the E_{rev} of I_{TRPML1} (+ 47 ± 2 mV, n = 3; see Suppl. fig. S3E). With cytoplasmic K^+, however, a small inward I_{TPC2} could be resolved with luminal isotonic Ca^{2+} (105 mM), but not $NMDG^+$ (Suppl. fig. S3B, D), suggesting a very limited Ca^{2+}

NIH-PA Author Manuscript

NIH-PA Author Manuscript

NIH-PA Author Manuscript

permeability for TPC2. By estimating the permeability ratios based on E_{rev} measurements, we determined the sequence of ion permeability or selectivity of I_{TPC2} as $Na^+ > Li^+ \gg Ca^{2+} \gg K^+ \sim Cs^+$ (Fig. 3C & Suppl. fig. S3F). P_{Ca}/P_{Na} and P_K/P_{Na} were about 0.10 and 0.03, respectively, which are similar to the values for canonical Na_V channels (0.08–0.11) (Favre et al., 1996; Hille, 1972). Consistent with the low P_K/P_{Na}, with a mixture of K^+ and Na^+ at both luminal and cytoplasmic sides, the Na^+-dependence of E_{rev} was fit with a Nernstian slope of 57 mV per 10-fold change of $[Na^+]_{cyto}$ (Fig. 3D). Taken together, these ion substitution analyses demonstrate that TPC2 is a highly Na^+-selective channel in the endolysosome.

Because the S4 segments of TPC1 and TPC2 contain several positively-charged amino acid residues, we investigated the voltage-dependence of I_{TPC}. Unlike canonical Na_V and Ca_V channels, I_{TPC} was not directly activated by membrane depolarization. Instead, in response to a step voltage protocol, PI(3,5)P_2-activated I_{TPC} inactivated at negative voltages (Suppl. fig. S3G), with I_{TPC1} exhibiting faster inactivation than I_{TPC2} (Fig. 3E). Inactivation recovered rapidly after a brief pulse to positive voltages (Suppl. fig. S3H). Despite being Na^+ selective, I_{TPC2} was insensitive to the Na_V blocker, TTX (Suppl. fig. S3I), but was sensitive to low concentrations of the nonselective Ca_V blocker, verapamil, in a voltage-dependent manner (Fig. 3F).

Na^+ is the major cation in the lysosome

The existence of Na^+-selective channels in the lysosome was unexpected because the lysosomal lumen, like the cytosol and the ER lumen (Morgan et al., 2011), has been presumed to contain high K^+ and low Na^+ (Morgan et al., 2011; Steinberg et al., 2010), suggesting the lack of a significant Na^+ or K^+ concentration gradient across the lysosomal membrane. To directly measure the ionic composition of the lysosome lumen, we enriched the lysosome fraction of HEK293T cells using density gradient centrifugation (Dong et al., 2010a; Graves et al., 2008b) (Suppl. fig. S4A; Fig. 4A), and then determined the ratios of major cations (Na^+, K^+, Ca^{2+}, and Mg^{2+}) using Inductively Coupled Plasma Mass Spectrometry (ICP-MS) analysis. All centrifugation steps were performed at 4 °C (1 h in the Percoll density gradient + 2.5 h in the iodixanol gradient; see Suppl. fig. S4A). At this temperature, the rate of ion transport across the lysosomal membrane is expected to be extremely low. In addition, the sucrose -based homogenization buffer contains few ions. Thus, lysosomal ion transporters/exchangers are not likely to be operative. Hence, we presume that the lysosomal ion composition is largely maintained during the isolation procedure. Similar approaches have been used to determine ionic compositions in a number of intracellular organelles, including mitochondria and synaptic vesicles (Cohn et al., 1968; Schmidt et al., 1980). Although the absolute concentrations of ions could not be accurately measured due to the lack of information about lysosome volume, this approach allowed us to determine the relative abundance/ratios of the total, but not free ions in the lumen. Interestingly, the K^+/Na^+ and Ca^{2+}/Na^+ ratios were only about 0.01 (Fig. 4B), which were not significantly affected by the trace amount of ions in the buffer (Suppl. fig. S4B). Similar results were obtained from human fibroblasts and mouse macrophages. Thus Na^+ is the predominant cation in the lumen of the lysosome (estimated to be ~ 140–150 mM, assuming that its lumen is iso-osmotic relative to the cytosol, and all the cations are osmotically-active) (Fig. 4B), indicating that in contrast to previous indirect measurements (Morgan et al., 2011; Steinberg et al., 2010), a large Na^+ concentration gradient is present across the lysosomal membrane.

To directly test whether the lysosomal lumen is a high Na^+-compartment, isolated lysosomes were treated with TPC agonists. Application of PI(3,5)P_2, but not PI(4,5)P_2, significantly increased the K^+/Na^+ ratios (Fig. 4C). Similarly, in isolated TPC2-mCherry lysosomes loaded with Sodium Green (Suppl. fig. S4C), a Na^+-sensitive dye (Carrithers et al., 2007),

NIH-PA Author Manuscript

NIH-PA Author Manuscript

NIH-PA Author Manuscript

$PI(3,5)P_2$, but not $PI(4,5)P_2$ application significantly decreased Sodium Green fluorescence (Fig. 4D). These results suggest that sustained activation of TPCs may reduce luminal Na^+ content. Consistent with the lysosome being a high Na^+ compartment rather than high K^+, when $PI(3,5)P_2$ was included in the pipette solution, a large I_{TPC2} was observed under the lysosome-attached configuration (Fig. 4E) in which the lysosomal content and hence the Na^+ gradient were maintained. Collectively, these results suggest that TPC-mediated Na^+ flux in response to a localized increase in $PI(3,5)P_2$ may rapidly depolarize endolysosomal membranes (luminal-side positive ~ + 30–110 mV at rest (Dong et al., 2010b; Morgan et al., 2011)), and facilitate membrane fusion (Suppl. fig. S4D). Consistently, TPC2-positive compartments were significantly enlarged in COS1 cells transfected with WT, but not D276K mutant hTPC2 (Suppl. fig. S4E, E′), suggesting that TPC2-expressing endolysosomes might have increased fusogenic potentials.

TPC1 and TPC2 underlie endogenous TPC-like currents in the endolysosome

Mice lacking *TPC1* or *TPC2* were generated and crossed to make double knockout ($TPC1^{-/-}/TPC2^{-/-}$) mice (Fig. 5A). In our targeting strategy, the first exons of the *TPC1* and *TPC2* genes were deleted, and the resulting recombinant transcripts failed to generate I_{TPC} (Suppl. fig. S5A). In vacuoles isolated from $TPC1^{-/-}/TPC2^{-/-}$ primary macrophages, $PI(3,5)P_2$ activated $I_{TRPML\text{-}L}$, but Na^+-selective (I_{TPC}-like; $I_{TPC\text{-}L}$) currents were absent (Fig. 5B). In contrast, $PI(3,5)P_2$ activated $I_{TPC\text{-}L}$ in the majority (> 90%) of vacuoles in *WT* (Fig. 5C) and $TRPML1^{-/-}$ (Fig. 1C) macrophages. The current amplitudes of $I_{TRPML\text{-}L}$ were not significantly different in $TPC1^{-/-}/TPC2^{-/-}$ compared to *WT* macrophages (Figs. 1B, 5B, 5D), but were dramatically reduced in $TRPML1^{-/-}$ macrophages (Figs. 1C, 5D). Although $I_{TRPML\text{-}L}$ and $I_{TPC\text{-}L}$ are both activated by $PI(3,5)P_2$, their I-V and E_{rev} differed significantly from each other. When we analyzed $PI(3,5)P_2$-activated currents at − 30 mV, large differences were noted between *WT,* $TRPML1^{-/-}$, and $TPC1^{-/-}/TPC2^{-/-}$ macrophages (Fig. 5E). Consistently, the $PI(3,5)P_2$-activated current was selective for Na^+ over Ca^{2+} (Suppl. fig. S5B). Collectively, these results suggest that $I_{TPC\text{-}L}$ is mediated by TPC2 and/or TPC1.

TPCs are not activated by NAADP

Since TPC1 and TPC2 were reportedly activated by NAADP in endolysosomes (Brailoiu et al., 2009; Calcraft et al., 2009; Morgan et al., 2011; Ruas et al., 2010; Zong et al., 2009), we measured endolysosomal currents after direct application of NAADP. Surprisingly, in TPC2-positive enlarged vacuoles, no significant current activation was seen with varying concentrations of NAADP (Fig. 6A; Suppl. fig. S6A). In contrast, $PI(3,5)P_2$ (10 μM) reliably (> 90%) and robustly activated I_{TPC2} in the same vacuoles. NAADP (1–10 μM) also failed to modulate or desensitize I_{TPC2} that was activated by a low concentration of $PI(3,5)P_2$ (100 nM; Fig. 6B). Similar results were seen with two NAADP analogs (4-methyl NAADP and 5-methyl NAADP) that induce Ca^{2+} release from sea urchin egg homogenates (Jain et al., 2010). I_{TPC1} was also insensitive to NAADP (Suppl. fig. S6A). To exclude the possibility that NAADP responsiveness was impaired in vacuolin-enlarged endolysosomes, we also tested NAADP on surface-expressed mutant hTPC2 channels (i.e. hTPC2-$L^{11}L^{12}$/AA; see ref. (Brailoiu et al., 2010)). However, plasma membrane I_{TPC2}, which exhibited no notable difference in channel properties to lysosomal I_{TPC2}, was also insensitive to NAADP in inside-out patches and in the whole-cell configuration (Fig. 6C, D). In contrast, NAADP (100 μM) activated NAADP-sensitive plasma membrane I_{TRPM2} (see ref. (Toth and Csanady, 2010)) (Suppl. fig. S6B, C), demonstrating that NAADP was active.

Pancreatic β–cells exhibit robust NAADP-mediated Ca^{2+} responses and have been commonly used as a cellular model to study endogenous NAADP signaling (Morgan et al., 2011). In INS1 pancreatic β-cell lines, intracellular perfusion with 100 nM NAADP in the whole-cell current-clamp configuration induced membrane depolarization and spike

NIH-PA Author Manuscript

NIH-PA Author Manuscript

NIH-PA Author Manuscript

generation (Fig. 7A). It has been reported that Ned-19, a membrane-permeable inhibitor of the NAADP receptor, completely inhibits NAADP- or glucose-induced Ca^{2+} responses at high μM concentrations (Naylor et al., 2009). However, Ned-19 had only a weak inhibitory effect on I_{hTPC2}, even at very high concentrations (1 mM; Suppl. fig. S6D). Together with the fact that TPCs have limited Ca^{2+} permeability, these results suggest that TPCs do not contribute directly to NAADP-induced endolysosomal Ca^{2+} release.

TPC currents are absent in pancreatic β-cell lines that exhibit NAADP-induced lysosomal Ca^{2+} release

Consistent with the results obtained from the pipette dialysis experiments (Fig. 7A), cell-permeant NAADP-AM (1–100 μM) (Parkesh et al., 2007) induced Ca^{2+} transients in INS1 (Fig. 7B, C; also see Suppl. fig. S7A, B) and MIN6 (see Suppl. fig. S7D) pancreatic β-cell lines, in the absence or presence of external Ca^{2+}. NAADP-AM-induced Ca^{2+} responses in INS-1 cells were abolished by the NAADP receptor blocker, Ned-19 (Fig. 7B, C & Suppl. fig. S7A), or by pretreatment with Bafilomycin A1, which inhibits V-ATPase to deplete acidic Ca^{2+} stores (Morgan et al., 2011) (Fig. 7C; also see Suppl. fig. S7C). These results suggest that, consistent with previous studies, NAADP induces Ca^{2+} release from lysosomal stores. Surprisingly, no measurable NAADP-activated whole-endolysosomal current was seen in INS1 (Fig. 7D; Suppl. fig. S7E) or MIN6 (Suppl. fig. S7F) cells. Furthermore, $PI(3,5)P_2$ (10 μM) activated $I_{TRPML\text{-}L}$ in 14/14 vacuoles, but I_X or $I_{TPC\text{-}L}$ were not detected (Fig. 7D & Suppl. fig. S7E, F). Collectively, NAADP-mediated responses appeared to be distinct from $I_{TPC\text{-}L}$ in pancreatic β-cell lines, suggesting that TPCs do not contribute to the NAADP-mediated response.

TPC1 and TPC2 are not required for NAADP- or glucose- induced Ca^{2+} responses in pancreatic islets

Glucose induces robust Ca^{2+} responses in pancreatic β-cells mediated via NAADP and its receptor localized in the endolysosome (Morgan et al., 2011; Naylor et al., 2009). However, in WT primary pancreatic β-cells, we did not observe significant whole-endolysosome $I_{TPC\text{-}L}$ (Fig. 7E). Glucose (5, 8, and 15 mM) induced significant increases of intracellular $[Ca^{2+}]$ (measured with Fura-2 Ca^{2+}-sensitive dyes) in pancreatic islets (Fig. 7F), which were dramatically inhibited by Ned-19 (100 μM; Fig. 7G), but the glucose-induced Ca^{2+} response was still largely intact in *TPC1*$^{-/-}$/*TPC2*$^{-/-}$ islets (Fig. 7F, G). Finally, the NAADP-AM-induced Ca^{2+} response was not significantly reduced in *TPC1*$^{-/-}$/*TPC2*$^{-/-}$ pancreatic islets (Fig. 7H). These results demonstrate that TPCs are not essential for NAADP- and glucose-induced Ca^{2+} responses in pancreatic β cells.

Discussion

TPCs have been reported to serve as the receptors (Brailoiu et al., 2009; Calcraft et al., 2009; Ruas et al., 2010; Zong et al., 2009) or co-receptors (Lin-Moshier et al., 2012) for NAADP, and NAADP-activated TPC currents were shown to be K^+-permeable (Pitt et al., 2010), Cs^+-permeable (Brailoiu et al., 2010), or Ca^{2+}-selective (Schieder et al., 2010). Those studies contrast drastically with our direct measurements of TPCs as NAADP-insensitive $PI(3,5)P_2$-activated Na^+-selective channels using whole-endolysosome patch-clamp recordings. Because NAADP-induced Ca^{2+} responses are robust in cells that lack $I_{TPC\text{-}L}$ and are largely intact in *TPC1*$^{-/-}$/*TPC2*$^{-/-}$ cells, and because our direct measurements of TPCs show that they are insensitive to NAADP, it should be clear that TPCs are not the NAADP receptor. Supporting this argument, recent studies using photoaffinity-labeled NAADP suggested that TPCs are unlikely to be the genuine NAADP binding sites (Lin-Moshier et al., 2012). Thus, the reported effects of TPCs on NAADP-induced Ca^{2+} release from endolysosomes (Morgan et al., 2011) could arise from indirect mechanisms, for example,

NIH-PA Author Manuscript

NIH-PA Author Manuscript

NIH-PA Author Manuscript

secondary to endolysosomal enlargement associated with TPC overexpression, or the change of the local Na^+ gradient across the lysosomal membrane. Given that we have not been able to detect any NAADP-activated whole-endolysosome current, it is also possible that vacuolin treatment could impair the detection of NAADP-sensitive conductance. On the other hand, one cannot rule out that NAADP, like Bafilomycin-A1 and Glycyl-L-phenylalanine 2-naphthylamide (GPN) (Morgan et al., 2011), might act via non-channel-mediated Ca^{2+} release mechanisms. NAADP might also target an unidentified anion conductance (low Cl^- recording solutions are used in the current study) to induce lysosomal Ca^{2+} release. Finally, NAADP might also induce Ca^{2+} release from non-lysosomal Ca^{2+} stores, but in a lysosome-dependent manner. Molecular identification of the NAADP-bound 22–23-kDa lysosomal proteins (Lin-Moshier et al., 2012) may help distinguish these possibilities.

The lysosomal lumen has been presumed to contain high K^+ and low Na^+ (Morgan et al., 2011; Steinberg et al., 2010), which would suggest the lack of a significant Na^+ or K^+ concentration gradient across the lysosomal membrane. These conclusions contrast directly with the high Na^+/low K^+ (like that of the extracellular media) we have found here using subcellular fractionation of organelles, which has been successfully applied to measure ionic compositions in a number of intracellular organelles, including mitochondria and synaptic vesicles (Cohn et al., 1968; Schmidt et al., 1980). Because the isolation procedures were performed at 4 °C using a homogenization buffer that limits ion exchange, the lysosomal ion composition is presumed to be largely maintained. Indeed, lysosome fractions prepared using this protocol are of relatively normal size (lysosome swelling could be caused by the loss of luminal ions) and are functional (Graves et al., 2008a; Radhakrishnan et al., 2008). Finally, the significant Na^+-selective current observed in the lysosome-attached configuration provides an independent verification that the lysosome lumen contains high concentrations of Na^+. It is worth mentioning that although a putative lysosomal K^+ release channel was proposed to provide counter ion flux for lysosomal acidification (Steinberg et al., 2010), such a scenario is unlikely to occur due to the high cytosolic K^+, hence the low or opposite electrochemical gradient of K^+ across the lysosome membrane. Instead, the existence of a large Na^+ gradient and lysosomal Na^+ channels are more likely to fulfill this function (counter-ion flux).

What is the purpose of Na^+ selective, $PI(3,5)P_2$-activated TPC channels? Increases in $PI(3,5)P_2$ will allow Na^+ to move down its concentration gradient, rapidly reducing and reversing (Suppl. Fig. S4D) the endolysosomal potential, which is presumed to be luminal-side positive at rest (estimated to be + 30 to + 110 mV) (Dong et al., 2010b). In model membranes, it has been demonstrated that Na^+ and K^+ exhibit differential effects on membrane curvature (Kraayenhof et al., 1996). While oppositely-charged lipid bilayers tend to fuse (Anzai et al., 1993), Na^+ influx into the cytoplasm reportedly affects membrane fusion during exocytosis (Parnas et al., 2000). Thus, TPC-mediated Na^+ flux in response to a localized increase in $PI(3,5)P_2$ may rapidly depolarize endolysosomal membranes and promote fusion (Suppl. Fig. S4D). Consistent with a previous study (Ruas et al., 2010), we found that TPC overexpression results in enlarged endolysosomes; this might be caused by enhanced endolysosomal fusion, decreased fission, or both. However, unlike TRPML1 (Shen et al., 2011), TPCs are not expressed in every cell type, suggesting that their role in membrane trafficking is more specific. Furthermore, because membrane fusion could occur even in *in vitro* reconstitution systems, neither TPCs nor TRPMLs are necessarily required as direct participants in the basic membrane fusion machinery (Shen et al., 2011). However, they may regulate the direction and specificity of lysosomal trafficking *in vivo*. Indeed, lysosomal trafficking is significantly delayed, although not blocked in cells lacking TRPML1 (Shen et al., 2011). Future research may reveal the relative importance of Na^+ *versus* Ca^{2+}, and TRPMLs *versus* TPCs in spatial and temporal regulation of lysosomal

NIH-PA Author Manuscript

NIH-PA Author Manuscript

NIH-PA Author Manuscript

trafficking. Finally, in addition to defining organelle specificity and determining the fusogenic potential of endolysosomes, the proposed cellular functions of $PI(3,5)P_2$ also include regulating endolysosomal ion homeostasis, especially H^+ homeostasis (Kerr et al., 2010; Shen et al., 2011). The proposed role of a putative monovalent cation (K^+ or Na^+) conductance in lysosomal acidification (Steinberg et al., 2010), together with our demonstration of a large Na^+ gradient across the endolysosomal membrane, suggest that $PI(3,5)P_2$-sensitive Na^+-permeable TPCs, but not K^+ release channels (see above), may participate in endolysosomal pH regulation in a transient and localized manner. In addition, rapid changes in Na^+ content will drive Na^+/H^+ exchangers in the organelle membrane, thus changing organellar pH. The exact sequence of events will depend on expanding our knowledge of transporters in endolysosomal membranes, and finding more accurate methods to measure endolysosomal potentials in intact cells.

Experimental Procedures

Targeted deletion of *TPC1* and *TPC2* in mice

TPC1 and *TPC2* double knockout mice were generated as described in Extended Experimental Procedures in the Supplementary Information.

Endolysosomal electrophysiology

Endolysosomal electrophysiology was performed in isolated enlarged endolysosomes using a modified patch-clamp method (Dong et al., 2010a). Cells were treated with 1 μM vacuolin-1, a lipid-soluble polycyclic triazine that can selectively increase the size of endosomes and lysosomes (Huynh and Andrews, 2005), for at least 1h, or up to 12h. Large vacuoles (up to 5 μm; capacitance = 1.1 ± 0.1 pF, n= 29 vacuoles) were observed in most vacuolin-treated cells. Occasionally, enlarged vacuoles were also seen in non-treated cells; no significant difference in TPC channel properties were seen for enlarged vacuoles obtained with or without vacuolin-1 treatment. Whole-endolysosome recordings were performed on manually isolated enlarged endolysosomes (Dong et al., 2010a). In brief, a patch pipette was pressed against a cell and quickly pulled away to slice the cell membrane. Enlarged endolysosomes were released into a dish and identified by monitoring EGFP-TPC1/2, mCherry-TPC1/2, or EGFP-Lamp1/mCherry-Lamp1 fluorescence. After formation of a gigaseal between the patch pipette and the enlarged endolysosome, capacitance transients were compensated. Voltage steps of several hundred mVs with ms duration were then applied to break into the vacuolar membrane (see Suppl. fig. S1). The whole-endolysosome configuration was verified by the re-appearance of capacitance transients after break-in (see Suppl. fig. S1).

Unless otherwise stated, bath (internal/cytoplasmic) solution contained (in mM) 140 K-gluconate, 4 NaCl, 1 EGTA, 2 $MgCl_2$, 0.39 $CaCl_2$, 20 HEPES (pH adjusted with KOH to 7.2; free $[Ca^{2+}]_i$ ~ 100 nM). In a subset of experiments, 2 mM Na_2-ATP and 0.1 mM GTP were added to the bath solution, and pH was re-adjusted. Pipette (luminal) solution was standard extracellular solution (modified Tyrode's; in mM): 145 NaCl, 5 KCl, 2 $CaCl_2$, 1 $MgCl_2$, 10 HEPES, 10 MES, 10 glucose (pH adjusted with NaOH to pH 4.6). In a subset of experiments, a low Cl^- pipette solution containing Na-gluconate replaced NaCl. All bath solutions were applied via a perfusion system that allowed us to achieve complete solution exchange within a few seconds. Data were collected using an Axopatch 2A patch clamp amplifier, Digidata 1440, and pClamp 10.2 software (Axon Instruments). Whole-endolysosome currents were digitized at 10 kHz and filtered at 2 kHz. All experiments were conducted at room temperature (21–23°C), and all recordings were analyzed with pClamp 10.2 and Origin 8.0 (OriginLab, Northampton, MA). All PIPs were from A.G. Scientific; water-soluble diC8-PIPs, prepared in high-concentration stock solutions, were dissolved in

NIH-PA Author Manuscript

NIH-PA Author Manuscript

NIH-PA Author Manuscript

the bath solutions, and delivered via the perfusion system at low concentrations (0.1–1 μM), and direct bath application at higher concentrations (10 μM). NAADP, 4-methyl NAADP, and 5-methyl NAADP were from Tocris Bioscience, Sigma, or kindly provided by Dr. Slama (Jain et al., 2010). The permeability to cations (relative to P_{Na}) was estimated based on E_{rev} measurement under bi-ionic conditions as described in Extended Experimental Procedures in the Supplementary Information.

Ca^{2+} imaging

Ca^{2+} imaging was performed using an EasyRatioPro system (PTI) as described in Extended Experimental Procedures in the Supplementary Information.

Lysosome isolation by subcellular fractionation

Lysosomes were isolated as described previously (Dong et al., 2010a; Graves et al., 2008b). Briefly, cell lysates were obtained by Dounce homogenization in a homogenizing buffer (HM buffer; 0.25 M sucrose, 1 mM EDTA, 10 mM HEPES, and pH 7.0), and then centrifuged at 1900 *g* (4, 200 rpm) at 4°C for 10 min to remove the nuclei and intact cells. Post-nuclear supernatants then underwent ultracentrifugation through a Percoll density gradient using a Beckman L8–70 ultracentrifuge. An ultracentrifuge tube was layered with 2.5 M sucrose, 18% Percoll in HM buffer. Centrifugation speed was 67,200 *g* (14,000 rpm) at 4°C for 1 h using a Beckman Coulter 70.1 Ti Rotor. Samples were fractionated into light, medium, and heavy membrane fractions. Heavy membrane fractions contained concentrated bands of cellular organelles and were further layered over a discontinuous iodixonal gradient. The iodixonal gradient was generated by mixing iodixonal in the HM buffer with 2.5 M glucose (in v/v; 27%, 22.5%, 19%, 16%, 12%, and 8%); the osmolarity of all solutions was ~ 300 mOsm. After centrifugation at 4°C for 2.5 h, the sample was divided into 10 fractions (0.5 ml each) for biochemical and atomic absorption analyses. Note that the ionic composition of the lysosome was largely maintained due to the low rate of ion transport across the lysosomal membrane at 4°C. Antibodies used for Western blots: anti-Lamp1 (Iowa Hybridoma bank), 1:5000 dilution; anti-Annexin V (Abcam), 1:2000 dilution; anti-GM130 (Abcam), 1:2000 dilution; anti-EEA1 (Santa Cruz Biotechnology), 1:500 dilution; anti-Complex II (Abcam), 1:5000 dilution; anti-GFP (Covance), 1:5000 dilution.

Inductively Coupled Plasma Mass Spectrometry (ICP-MS)

Lysosomal fractions were prepared for atomic absorption by diluting the samples in a 1:1 ratio with concentrated nitric acid. After digestion (10min, 60°C), the ionic composition was measured using a Thermo Scientific Finnigan Element inductively coupled with a plasma-high resolution mass spectrometer (ICP-HRMS)(Seby et al., 2003).

Data analysis

Data are presented as the mean ± standard error of the mean (SEM). Statistical comparisons were made using analysis of variance (ANOVA). A P value < 0.05 was considered statistically significant.

Supplementary Material

Refer to Web version on PubMed Central for supplementary material.

Acknowledgments

This work was supported by NIH RO1 grants (NS062792 to H.X., NS055293 to D.R., GM081658 to M.X.Z., and HHMI to D.C.) and a Sloan Research Fellowship (to H.X). We thank the Gene Manipulation Facility of the

NIH-PA Author Manuscript

NIH-PA Author Manuscript

NIH-PA Author Manuscript

Children's Hospital Boston (*TPC1*) and the Transgenic & Chimera Mouse Facility at the University of Pennsylvania (*TPC2*) for ES cell injection.

References

Anzai K, Masumi M, Kawasaki K, Kirino Y. Frequent fusion of liposomes to a positively charged planar bilayer without calcium ions. J Biochem. 1993; 114:487–491. [PubMed: 7506250]

Brailoiu E, Churamani D, Cai X, Schrlau MG, Brailoiu GC, Gao X, Hooper R, Boulware MJ, Dun NJ, Marchant JS, et al. Essential requirement for two-pore channel 1 in NAADP-mediated calcium signaling. J Cell Biol. 2009; 186:201–209. [PubMed: 19620632]

Brailoiu E, Rahman T, Churamani D, Prole DL, Brailoiu GC, Hooper R, Taylor CW, Patel S. An NAADP-gated Two-pore Channel Targeted to the Plasma Membrane Uncouples Triggering from Amplifying Ca2+ Signals. J Biol Chem. 2010; 285:38511–38516. [PubMed: 20880839]

Calcraft PJ, Ruas M, Pan Z, Cheng X, Arredouani A, Hao X, Tang J, Rietdorf K, Teboul L, Chuang KT, et al. NAADP mobilizes calcium from acidic organelles through two-pore channels. Nature. 2009; 459:596–600. [PubMed: 19387438]

Carrithers MD, Dib-Hajj S, Carrithers LM, Tokmoulina G, Pypaert M, Jonas EA, Waxman SG. Expression of the voltage-gated sodium channel NaV1.5 in the macrophage late endosome regulates endosomal acidification. J Immunol. 2007; 178:7822–7832. [PubMed: 17548620]

Chow CY, Zhang Y, Dowling JJ, Jin N, Adamska M, Shiga K, Szigeti K, Shy ME, Li J, Zhang X, et al. Mutation of FIG4 causes neurodegeneration in the pale tremor mouse and patients with CMT4J. Nature. 2007; 448:68–72. [PubMed: 17572665]

Cohn DV, Bawdon R, Newman RR, Hamilton JW. Effect of calcium chelation on the ion content of liver mitochondria in carbon tetrachloride-poisoned rats. J Biol Chem. 1968; 243:1089–1095. [PubMed: 4967139]

Dong XP, Shen D, Wang X, Dawson T, Li X, Zhang Q, Cheng X, Zhang Y, Weisman LS, Delling M, et al. PI(3,5)P(2) Controls Membrane Traffic by Direct Activation of Mucolipin Ca Release Channels in the Endolysosome. Nat Commun. 2010a:1.

Dong XP, Wang X, Xu H. TRP channels of intracellular membranes. J Neurochem. 2010b; 113:313–328. [PubMed: 20132470]

Dove SK, Dong K, Kobayashi T, Williams FK, Michell RH. Phosphatidylinositol 3,5-bisphosphate and Fab1p/PIKfyve underPPIn endo-lysosome function. Biochem J. 2009; 419:1–13. [PubMed: 19272020]

Favre I, Moczydlowski E, Schild L. On the structural basis for ionic selectivity among Na+, K+, and Ca2+ in the voltage-gated sodium channel. Biophys J. 1996; 71:3110–3125. [PubMed: 8968582]

Graves AR, Curran PK, Smith CL, Mindell JA. The Cl−/H+ antiporter ClC-7 is the primary chloride permeation pathway in lysosomes. Nature. 2008a; 453:788–792. [PubMed: 18449189]

Graves AR, Curran PK, Smith CL, Mindell JA. The Cl(−)/H(+) antiporter ClC-7 is the primary chloride permeation pathway in lysosomes. Nature. 2008b

Grimm C, Jors S, Saldanha SA, Obukhov AG, Pan B, Oshima K, Cuajungco MP, Chase P, Hodder P, Heller S. Small molecule activators of TRPML3. Chem Biol. 2010; 17:135–148. [PubMed: 20189104]

Guse AH. Second messenger signaling: multiple receptors for NAADP. Curr Biol. 2009; 19:R521–523. [PubMed: 19602416]

Hille B. The permeability of the sodium channel to metal cations in myelinated nerve. J Gen Physiol. 1972; 59:637–658. [PubMed: 5025743]

Huynh C, Andrews NW. The small chemical vacuolin-1 alters the morphology of lysosomes without inhibiting Ca2+-regulated exocytosis. EMBO Rep. 2005; 6:843–847. [PubMed: 16113649]

Jain P, Slama JT, Perez-Haddock LA, Walseth TF. Nicotinic acid adenine dinucleotide phosphate analogues containing substituted nicotinic acid: effect of modification on Ca(2+) release. J Med Chem. 2010; 53:7599–7612. [PubMed: 20942470]

Kerr MC, Wang JT, Castro NA, Hamilton NA, Town L, Brown DL, Meunier FA, Brown NF, Stow JL, Teasdale RD. Inhibition of the PtdIns(5) kinase PIKfyve disrupts intracellular replication of Salmonella. EMBO J. 2010; 29:1331–1347. [PubMed: 20300065]

NIH-PA Author Manuscript

NIH-PA Author Manuscript

NIH-PA Author Manuscript

Kraayenhof R, Sterk GJ, Wong Fong Sang HW, Krab K, Epand RM. Monovalent cations differentially affect membrane surface properties and membrane curvature, as revealed by fluorescent probes and dynamic light scattering. Biochim Biophys Acta. 1996; 1282:293–302. [PubMed: 8703985]

Lange I, Yamamoto S, Partida-Sanchez S, Mori Y, Fleig A, Penner R. TRPM2 functions as a lysosomal Ca2+-release channel in beta cells. Sci Signal. 2009; 2:ra23. [PubMed: 19454650]

Lin-Moshier Y, Walseth TF, Churamani D, Davidson SM, Slama JT, Hooper R, Brailoiu E, Patel S, Marchant JS. Photoaffinity Labeling of Nicotinic Acid Adenine Dinucleotide Phosphate (NAADP) Targets in Mammalian Cells. J Biol Chem. 2012; 287:2296–2307. [PubMed: 22117075]

Morgan AJ, Platt FM, Lloyd-Evans E, Galione A. Molecular mechanisms of endolysosomal Ca2+ signalling in health and disease. Biochem J. 2011; 439:349–374. [PubMed: 21992097]

Naylor E, Arredouani A, Vasudevan SR, Lewis AM, Parkesh R, Mizote A, Rosen D, Thomas JM, Izumi M, Ganesan A, et al. Identification of a chemical probe for NAADP by virtual screening. Nat Chem Biol. 2009; 5:220–226. [PubMed: 19234453]

Nilius B, Owsianik G, Voets T. Transient receptor potential channels meet phosphoinositides. EMBO J. 2008; 27:2809–2816. [PubMed: 18923420]

Parkesh R, Lewis AM, Aley PK, Arredouani A, Rossi S, Tavares R, Vasudevan SR, Rosen D, Galione A, Dowden J, et al. Cell-permeant NAADP: A novel chemical tool enabling the study of Ca(2+) signalling in intact cells. Cell Calcium. 2007

Parnas H, Segel L, Dudel J, Parnas I. Autoreceptors, membrane potential and the regulation of transmitter release. Trends Neurosci. 2000; 23:60–68. [PubMed: 10652546]

Pitt SJ, Funnell TM, Sitsapesan M, Venturi E, Rietdorf K, Ruas M, Ganesan A, Gosain R, Churchill GC, Zhu MX, et al. TPC2 is a novel NAADP-sensitive Ca2+ release channel, operating as a dual sensor of luminal pH and Ca2+ J Biol Chem. 2010; 285:35039–35046. [PubMed: 20720007]

Radhakrishnan A, Goldstein JL, McDonald JG, Brown MS. Switch-like control of SREBP-2 transport triggered by small changes in ER cholesterol: a delicate balance. Cell Metab. 2008; 8:512–521. [PubMed: 19041766]

Ruas M, Rietdorf K, Arredouani A, Davis LC, Lloyd-Evans E, Koegel H, Funnell TM, Morgan AJ, Ward JA, Watanabe K, et al. Purified TPC Isoforms Form NAADP Receptors with Distinct Roles for Ca(2+) Signaling and Endolysosomal Trafficking. Curr Biol. 2010

Schieder M, Rotzer K, Bruggemann A, Biel M, Wahl-Schott CA. Characterization of two-pore channel 2 (TPCN2)-mediated Ca2+ currents in isolated lysosomes. J Biol Chem. 2010; 285:21219–21222. [PubMed: 20495006]

Schmidt R, Zimmermann H, Whittaker VP. Metal ion content of cholinergic synaptic vesicles isolated from the electric organ of Torpedo: effect of stimulation-induced transmitter release. Neuroscience. 1980; 5:625–638. [PubMed: 7374962]

Seby F, Gagean M, Garraud H, Castetbon A, Donard OF. Development of analytical procedures for determination of total chromium by quadrupole ICP-MS and high-resolution ICP-MS, and hexavalent chromium by HPLC-ICP-MS, in different materials used in the automotive industry. Anal Bioanal Chem. 2003; 377:685–694. [PubMed: 12904954]

Shen D, Wang X, Xu H. Pairing phosphoinositides with calcium ions in endolysosomal dynamics: Phosphoinositides control the direction and specificity of membrane trafficking by regulating the activity of calcium channels in the endolysosomes. Bioessays. 2011; 33:448–457. [PubMed: 21538413]

Steinberg BE, Huynh KK, Brodovitch A, Jabs S, Stauber T, Jentsch TJ, Grinstein S. A cation counterflux supports lysosomal acidification. J Cell Biol. 2010; 189:1171–1186. [PubMed: 20566682]

Suh BC, Hille B. PIP2 is a necessary cofactor for ion channel function: how and why? Annu Rev Biophys. 2008; 37:175–195. [PubMed: 18573078]

Sulem P, Gudbjartsson DF, Stacey SN, Helgason A, Rafnar T, Jakobsdottir M, Steinberg S, Gudjonsson SA, Palsson A, Thorleifsson G, et al. Two newly identified genetic determinants of pigmentation in Europeans. Nat Genet. 2008; 40:835–837. [PubMed: 18488028]

Toth B, Csanady L. Identification of direct and indirect effectors of the transient receptor potential melastatin 2 (TRPM2) cation channel. J Biol Chem. 2010; 285:30091–30102. [PubMed: 20650899]

NIH-PA Author Manuscript

NIH-PA Author Manuscript

NIH-PA Author Manuscript

Yamasaki M, Masgrau R, Morgan AJ, Churchill GC, Patel S, Ashcroft SJ, Galione A. Organelle selection determines agonist-specific Ca2+ signals in pancreatic acinar and beta cells. J Biol Chem. 2004; 279:7234–7240. [PubMed: 14660554]

Yu FH, Catterall WA. The VGL-chanome: a protein superfamily specialized for electrical signaling and ionic homeostasis. Sci STKE. 2004; 2004:re15. [PubMed: 15467096]

Zong X, Schieder M, Cuny H, Fenske S, Gruner C, Rotzer K, Griesbeck O, Harz H, Biel M, Wahl-Schott C. The two-pore channel TPCN2 mediates NAADP-dependent Ca(2+)-release from lysosomal stores. Pflugers Arch. 2009; 458:891–899. [PubMed: 19557428]

NIH-PA Author Manuscript

NIH-PA Author Manuscript

NIH-PA Author Manuscript

- TPC proteins are sodium-selective channels in the lysosome.
- TPC channels are activated specifically by $PI(3,5)P_2$.
- TPC channels are not NAADP receptors.
- Lysosomes are high sodium compartments.

NIH-PA Author Manuscript
NIH-PA Author Manuscript
NIH-PA Author Manuscript

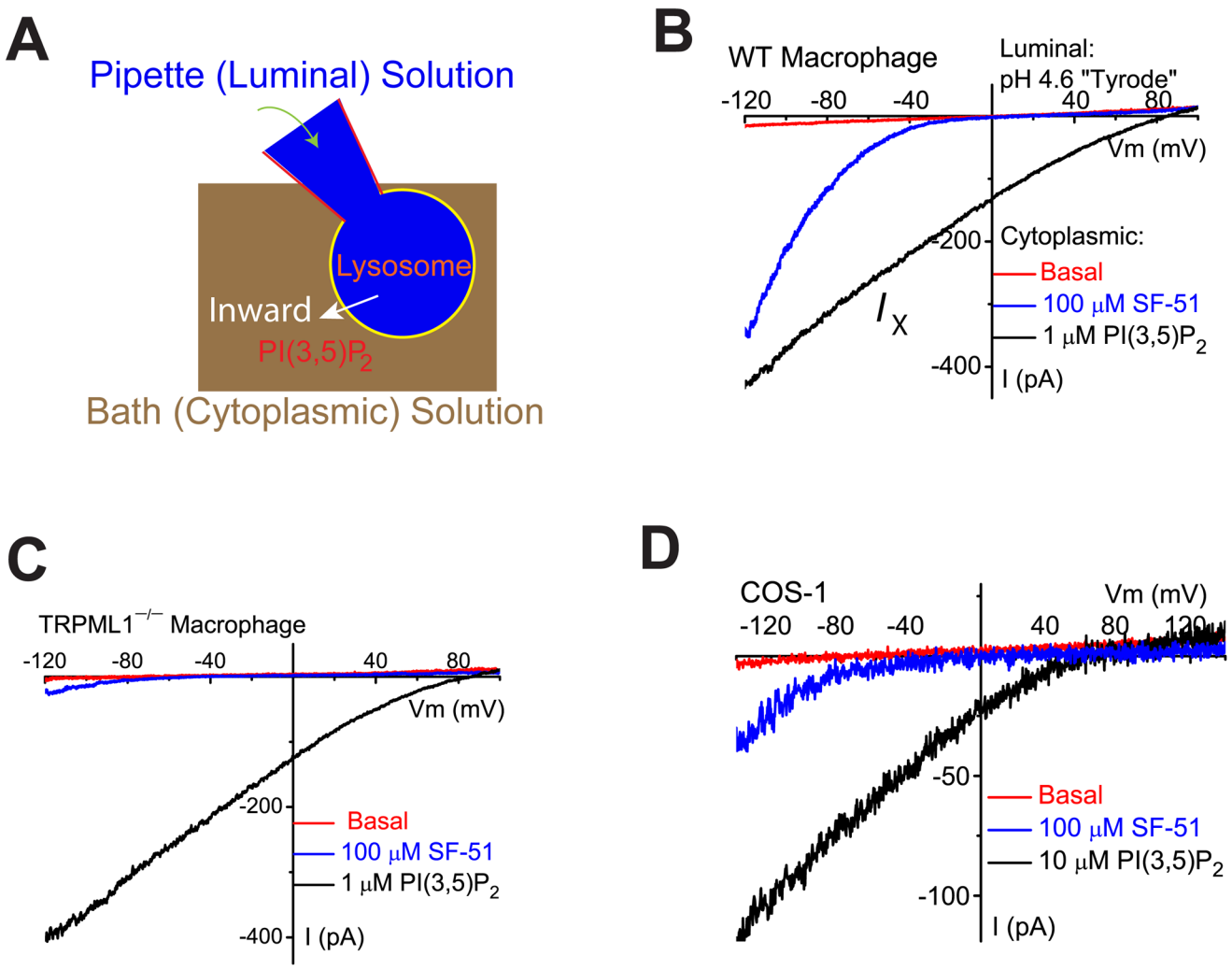

Figure 1. $PI(3,5)P_2$ activates endogenous TRPML1-independent inward currents in endolysosomes

(A). Illustration of the whole-endolysosome recording configuration. Pipette (luminal) solution was a standard external (modified Tyrode's) solution adjusted to pH 4.6 to mimic the acidic environment of the lysosomal lumen. Bath (internal/cytoplasmic) solution was a K^+-based internal solution (140 mM K^+-gluconate). Note that the inward current indicates cations flowing out of the endolysosome (arrow). **(B).** Bath application of $PI(3,5)P_2$ (diC8, 1 μM) to the cytoplasmic side of enlarged endolysosome/vacuoles isolated from vacuolin-treated *WT* primary macrophage cells activated whole-endolysosome currents (296 ± 28pA/pF at −120mV, n = 24 vacuoles/endolysosomes) with positive E_{rev} (79 ± 2.4mV, n = 20). K^+-based cytoplasmic/bath solution contained (in mM) $140K^+/4Na^+/2Mg^{2+}$ (pH 7.2, free Ca^{2+} ~ 100 nM); luminal/pipette solution was a pH 4.6 modified Tyrode solution, which contained (in mM) $145Na^+/5K^+/1Mg^{2+}/2\ Ca^{2+}$ (pH 4.6); the equilibrium potential of Na^+ (E_{Na}) was estimated to be ~ +90mV. Inwardly rectifying TRPML-like currents ($I_{TRPML\text{-}L}$) with E_{rev} = 3.7 ± 1.7 mV (n = 20) were induced by a TRPML-specific small molecule agonist (SF-51) in the same vacuoles (blue trace). **(C).** $PI(3,5)P_2$ activated a current with a positive E_{rev} in an enlarged endolysosome/vacuole isolated from a $TRPML1^{-/-}$ primary macrophage cell. **(D).** $PI(3,5)P_2$ (10 μM) activated whole-endolysosome current (from 30 to 420 pA measured at −120 mV) with positive E_{rev} in enlarged endolysosome/vacuoles

isolated from non-transfected COS-1 cells. Note the small $I_{TRPML\text{-}L}$ (E_{rev} ~ 0mV) activated by SF-51 in the same vacuoles. Data are presented as the mean ± standard error of the mean (SEM). See also Figure S1.

NIH-PA Author Manuscript
NIH-PA Author Manuscript
NIH-PA Author Manuscript

NIH-PA Author Manuscript

NIH-PA Author Manuscript

NIH-PA Author Manuscript

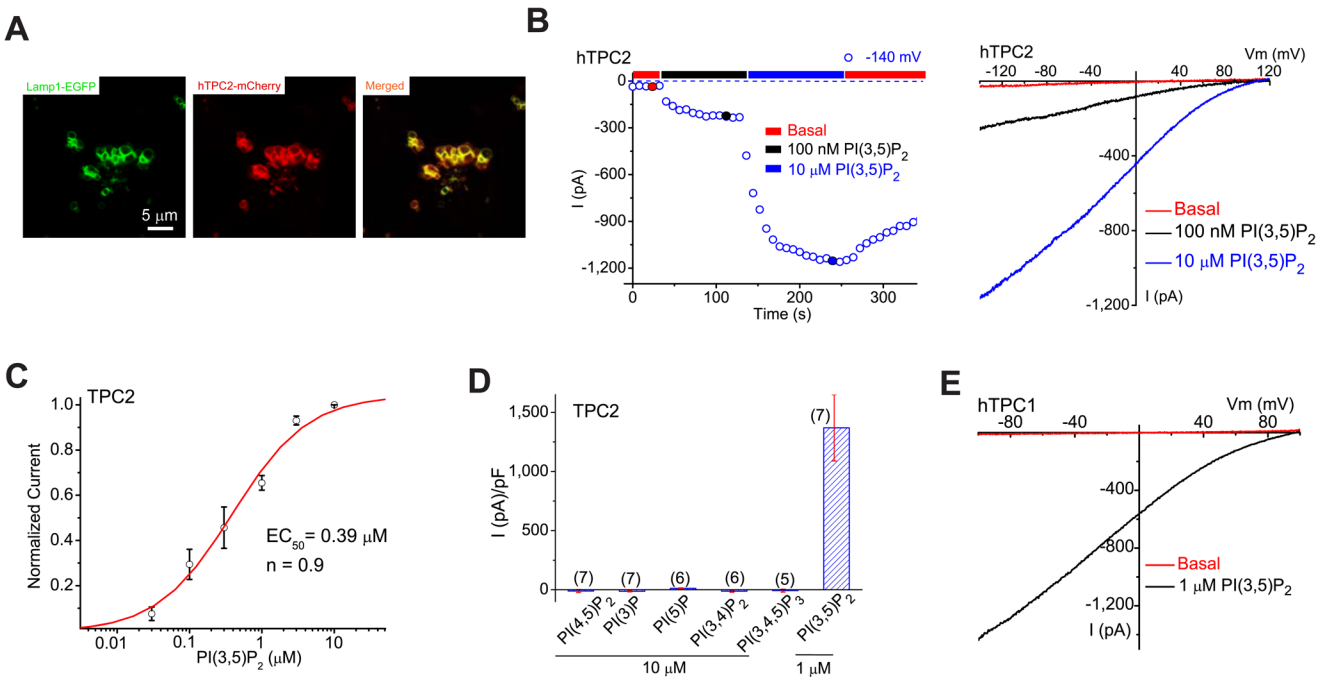

Figure 2. PI(3,5)P_2 activates recombinant TPCs in endolysosomes

(A). TPC2 proteins are localized in Lamp1-positive late endosomes and lysosomes in COS-1 cells that were transfected with TPC2 and Lamp-1 fusion proteins and treated with vacuolin-1. **(B).** PI(3,5)P_2 activated a large whole-endolysosome current with E_{rev} > + 80mV in an EGFP (hTPC2)-positive endolysosome isolated from an *hTPC2-EGFP*-transfected COS-1 cell. Whole-endolysosome currents were elicited by repeated voltage ramps (−140 to +140 mV; 400 ms) with a 4s interval between ramps; current amplitudes measured at −140 mV were used to plot the time course of activation. The right panel shows representative I-V traces of hTPC2-mediated whole-endolysosome currents (I_{hTPC2}) before (red; −20 ± 4pA/pF at −120 mV, n = 9) and after (black and blue) PI(3,5)P_2 bath application at three different time points, as indicated in the left panel (red, blue and black circles). Only a portion of the voltage protocol is shown; holding potential (HP) = 0 mV. **(C).** Dose-dependence of PI(3,5)P_2-dependent activation (EC_{50} = 390 ± 94 nM, Hill slope (n) = 0.9, n= 13 vacuoles). **(D).** Specific activation of TPC2 by PI(3,5)P_2 (in 1 μM), but not other PIPs (all in 10 μM). On average, I_{TPC2} in the presence of 1μM PI(3,5)P_2 was 1410 ± 360pA/pF at −120mV (n = 7). **(E).** Activation of I_{hTPC1} by 1 μM PI(3,5)P_2. Data are presented as the mean ± SEM. See also Figure S2.

NIH-PA Author Manuscript

NIH-PA Author Manuscript

NIH-PA Author Manuscript

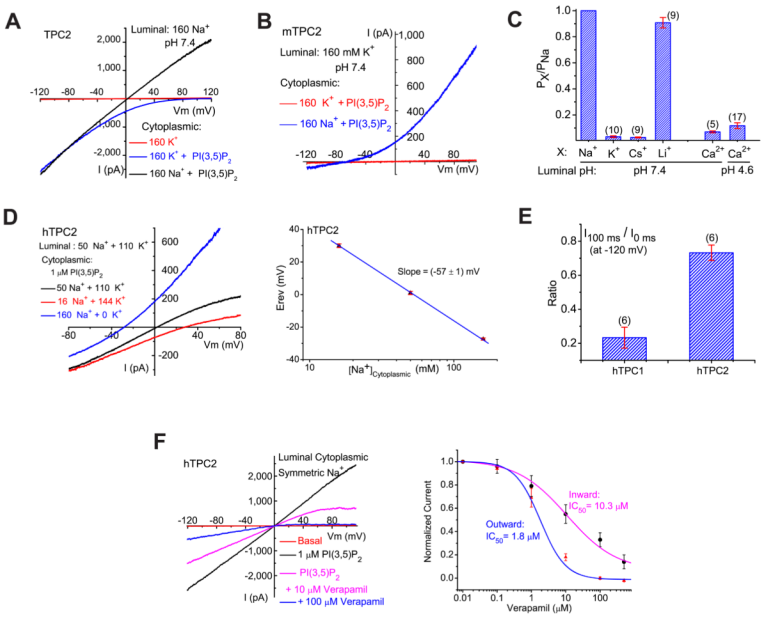

Figure 3. PI(3,5)P_2-activated TPC currents are Na^+-selective

(A). PI(3,5)P_2-activated I_{TPC2} (E_{rev}= + 89 mV ± 5mV, n = 8) under bi-ionic conditions with luminal/pipette Na^+ and cytoplasmic/bath K^+. Large outward I_{hTPC2} was observed in cytoplasmic Na^+. (**B).** I_{mTPC2} E_{rev} (−68 ± 3mV, n = 5) under bi-ionic conditions with luminal K^+ and cytoplasmic Na^+. (**C**). Relative cationic permeability ratios of I_{hTPC2} based on E_{rev} measurement under bi-ionic conditions. (**D).** Na^+-dependence of I_{hTPC2} E_{rev}. The left panel shows I-V relations of I_{hTPC2} with cytoplasmic solutions containing various concentrations of Na^+ and K^+. (**E).** Distinct inactivation kinetics of I_{hTPC2} and I_{hTPC1} at −120 mV. (**F).** Verapamil inhibited outward and inward I_{hTPC2} with different dose-dependencies under luminal and cytoplasmic symmetric Na^+ (luminal pH 7.4). Data are presented as the mean ± SEM. See also Figure S3.

NIH-PA Author Manuscript
NIH-PA Author Manuscript
NIH-PA Author Manuscript

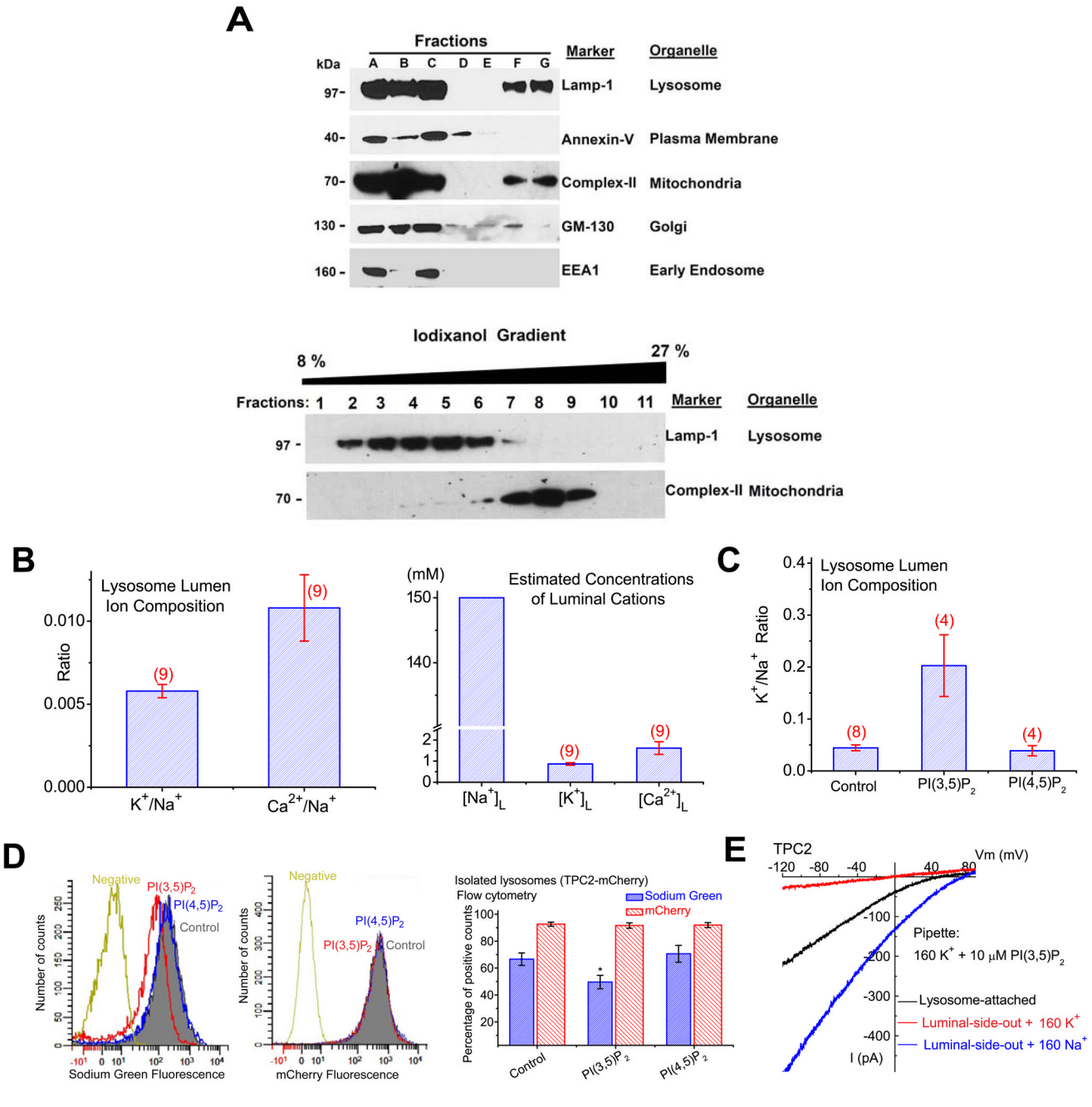

Figure 4. Na^+ is the major cation in the lysosome

(A). Western blotting was performed for each fraction (A–G) using various organelle markers: Lamp-1 for the lysosome; annexin-V for the plasma membrane; complex II for the mitochondria; GM-130 for the Golgi; EEA1 for the early endosome. Cellular fractionation protocol is described in Suppl. Fig. S4. Centrifugation of cell homogenate (fraction A) of HEK293T cells resulted in a pellet (fraction B) and a supernatant (fraction C). The supernatant was then layered over a discontinued gradient containing a cushion of 2.5 M sucrose and 18% Percoll in the HM buffer. Further centrifugation of the gradient resulted in the light membrane fraction (fraction D), the medium membrane fraction (fraction E), and the heavy membrane fraction (fraction G). Lower panel: fraction G was then layered over a

NIH-PA Author Manuscript

NIH-PA Author Manuscript

NIH-PA Author Manuscript

discontinuous iodixonal (8–27%) gradient (fractions 1–11); Western blotting was performed for each fraction using Anti-Lamp-1 and Anti- complex II. **(B)**. Ionic composition (Na^+, K^+, and Ca^{2+}) in the lysosomal lumen of HEK293T cells determined by Inductively Coupled Plasma Mass Spectrometry (ICP-MS). Right panel: estimated concentrations of Na^+, K^+, and Ca^{2+} in the lysosome lumen; estimates were based on the assumptions that the lysosome lumen is iso-osmotic relative to the cytosol, and all the cations are osmotically-active. **(C)**. Luminal K^+/Na^+ ratios were significantly increased for isolated lysosomes that were treated with $PI(3,5)P_2$ (20 μM), but not $PI(4,5)P_2$ (20 μM). **(D)**. Left panel: application of $PI(3,5)P_2$ (red), but not $PI(4,5)P_2$ (blue) to isolated lysosomes decreased Sodium Green, but not mCherry fluorescence. Lysosomes were isolated from TPC2-mCherry-expressing HEK293 cells and loaded with Sodium Green dyes. “Control” and “Negative” indicate fluorescence levels in isolated lysosomes with and without Sodium Green dye loading, respectively. Right panel: decreased Sodium Green fluorescence intensity (reflecting luminal Na^+ concentration) from $PI(3,5)P_2$-treated lysosomes; data are presented as the percentage of lysosomes that were Sodium Green-positive. mCherry fluorescence remained constant upon $PI(3,5)P_2$/$PI(4,5)P_2$ application. **(E)**. I_{TPC2} measured in lysosome-attached configuration. I_{TPC2} was activated in the lysosome-attached configuration with $PI(3,5)P_2$ (10 μM) in the K^+ pipette solution. I_{TPC2} was detected with luminal Na^+, but not K^+ upon excision into the luminal-side-out configuration. Note that the indicated voltages in the lysosome-attached configuration contained a contribution from the lysosomal membrane potential, for which no accurate measurement is available. The smaller current amplitude seen in the lysosome-attached configuration might be due to luminal [Na^+] lower than 160 mM, relief from luminal inhibition, or both. Data are presented as the mean ± SEM. See also Figure S4.

NIH-PA Author Manuscript

NIH-PA Author Manuscript

NIH-PA Author Manuscript

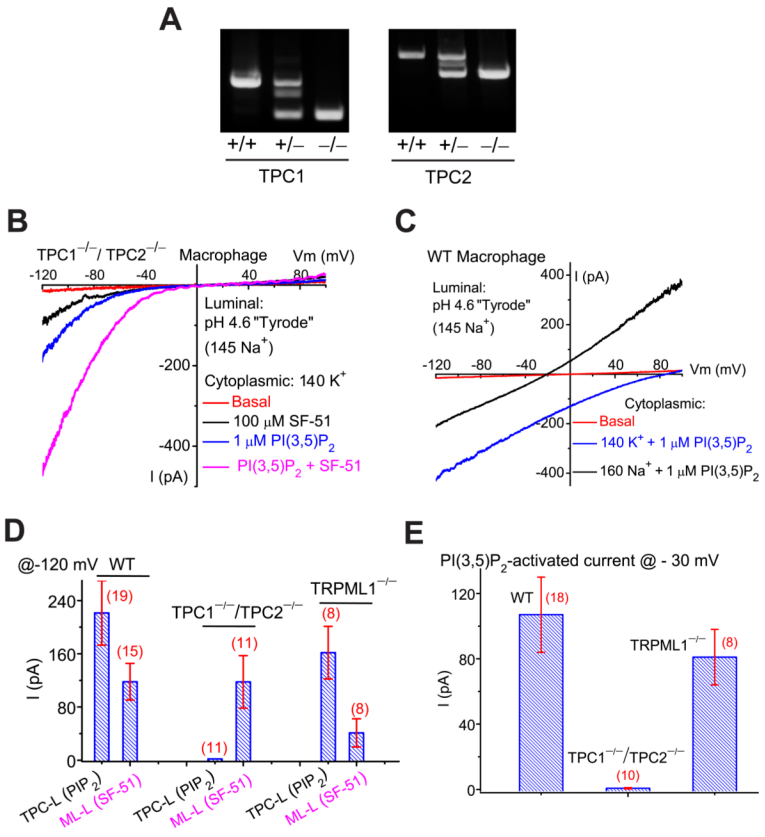

Figure 5. Genetic inactivation of TPC1 and TPC2 abolishes TPC currents in the endolysosome

(A). PCR genotyping of *TPC1 KO (TPC1*$^{-/-}$*)* and *TPC2 KO (TPC2*$^{-/-}$*)* mice. **(B).** Lack of significant PI(3,5)P_2-activated TPC-like current ($I_{TPC\text{-}L}$) in vacuoles isolated from a *TPC1*$^{-/-}$*/TPC2*$^{-/-}$ mouse macrophage. Instead, in 15/15 vacuoles, PI(3,5)P_2 activated $I_{TRPML\text{-}L}$ that was further potentiated by SF-51. **(C).** An endogenous $I_{TPC\text{-}L}$ activated by PI(3,5)P_2 (1 μM) in a vacuole isolated from a *WT* mouse macrophage cell. Switching the cytoplasmic solution from K^+ to Na^+ resulted in a leftward shift of E_{rev}, and an increase of the current in the outward direction. **(D).** Summary of $I_{TPC\text{-}L}$ and $I_{TRPML\text{-}L}$ in *WT, TPC1*$^{-/-}$*/TPC2*$^{-/-}$, and *TRPML1*$^{-/-}$ macrophages. (**E).** Summary of PI(3,5)P_2-activated whole-endolysosome inward currents in *WT, TPC1*$^{-/-}$*/TPC2*$^{-/-}$, and *TRPML1*$^{-/-}$ macrophages at −30mV. I_{PIP2} was 107 ± 23pA/pF (n= 18) and 0.7 ± 0.4pA/pF (n=10) for *WT* and *TPC1*$^{-/-}$*/TPC2*$^{-/-}$ macrophages, respectively. Data are presented as the mean ± SEM. See also Figure S5.

NIH-PA Author Manuscript
NIH-PA Author Manuscript
NIH-PA Author Manuscript

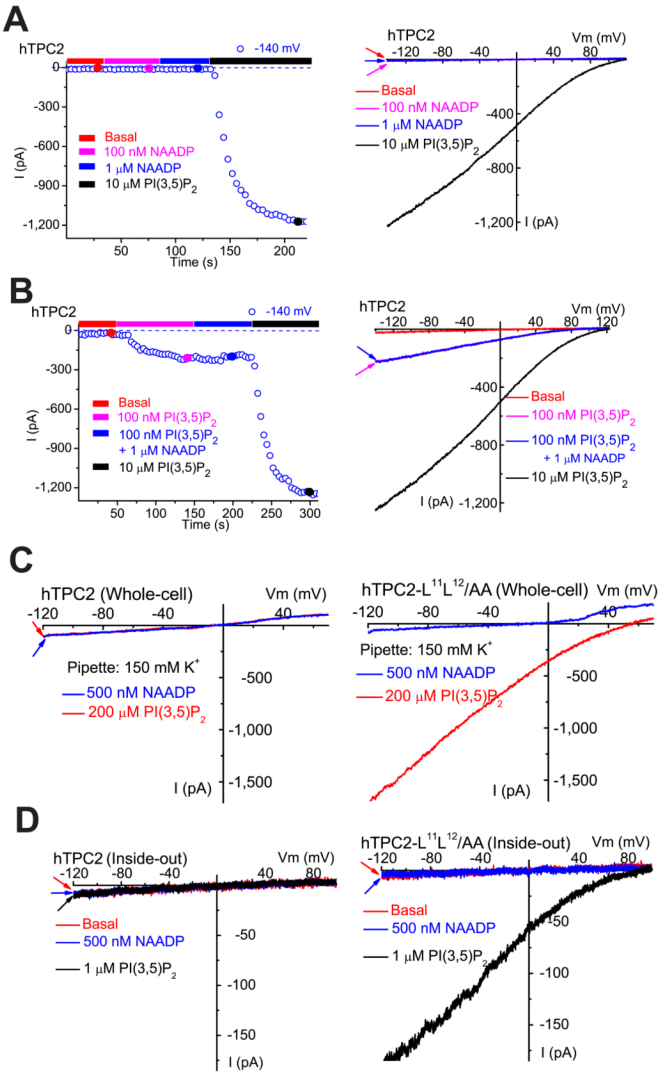

Figure 6. NAADP does not activate TPCs

(A). NAADP (100 nM or 1 μM) failed to activate whole-endolysosome I_{hTPC2}. In contrast, $PI(3,5)P_2$ robustly activated I_{hTPC2} in the same vacuole. The right panel shows representative I-V traces of whole-endolysosome currents at 4 different time points (indicated by color-coded circles) shown in the left panel. **(B)**. NAADP (1 μM) failed to modulate $PI(3,5)P_2$–activated I_{hTPC2}. **(C).** Pipette dialysis of $PI(3,5)P_2$ (200 μM) or NAADP (500 nM) failed to elicit whole-cell current in HEK293T cells transfected with WT hTPC2. In contrast, pipette dialysis of $PI(3,5)P_2$ (200 μM), but not NAADP (500 nM), activated whole-cell I_{TPC2} in HEK293T cells transfected with a surface-expressed hTPC2 mutant (hTPC2-$L^{11}L^{12}$/AA). **(D).** $PI(3,5)P_2$, but not NAADP, activated $I_{TPC2\text{-}LL\text{-}AA}$ in inside-out macro-patches isolated from hTPC2-$L^{11}L^{12}$/AA -transfected HEK293T cells. Data are presented as the mean ± SEM. See also Figure S6.

NIH-PA Author Manuscript
NIH-PA Author Manuscript
NIH-PA Author Manuscript

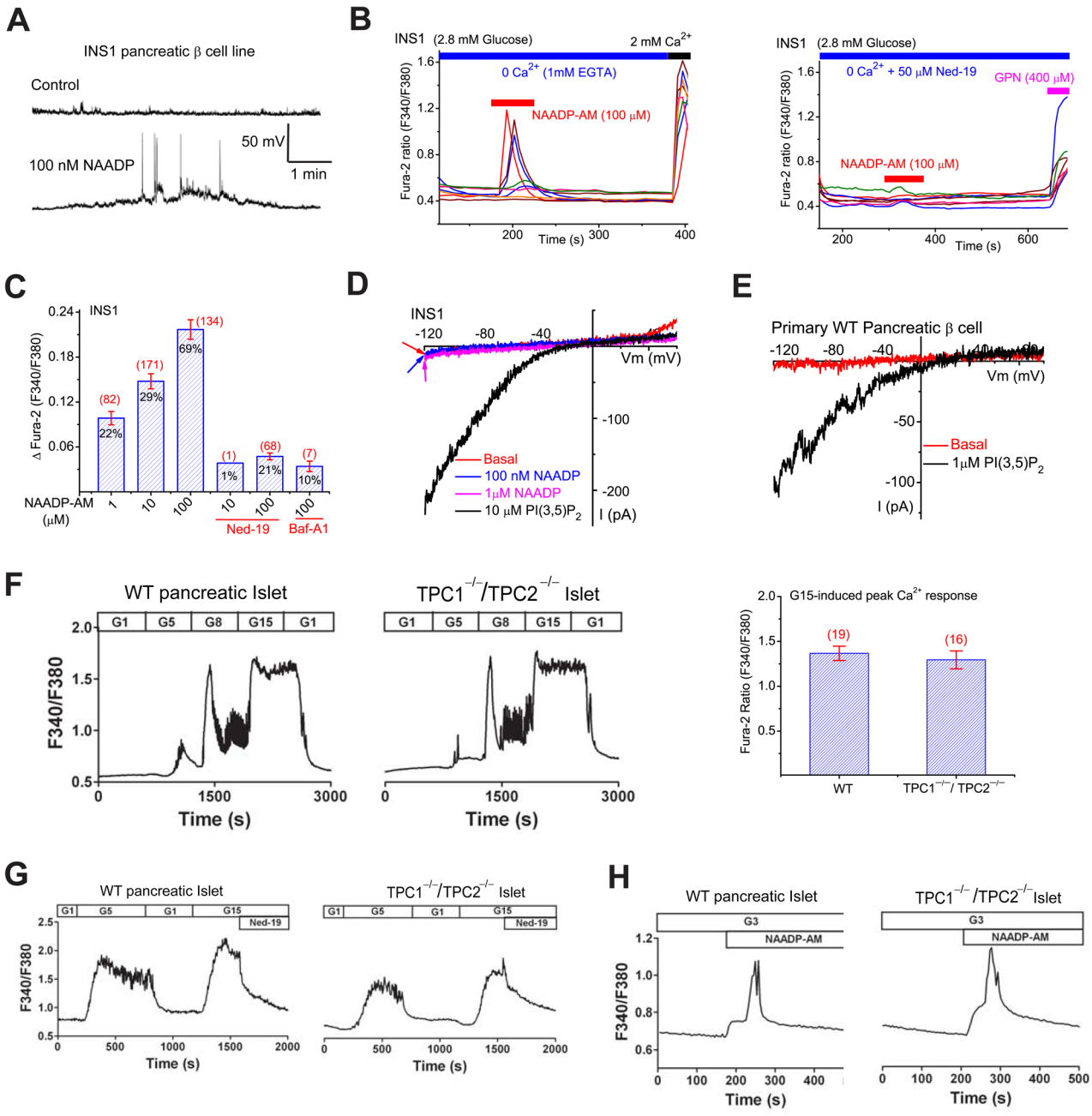

Figure 7. NAADP induces lysosomal Ca^{2+} release in cells that lack TPC currents or proteins

(A). Pipette dialysis of NAADP (100 nM) induced membrane depolarization and spike generation in an INS1 pancreatic β-cell line under the whole-cell current-clamp configuration. **(B).** In the absence of external Ca^{2+} (free $[Ca^{2+}] < 10$ nM), NAADP-AM (100 μM) induced Ca^{2+} release measured with Fura-2 (F_{340}/F_{380}) ratios from intracellular stores in INS1 cells; Ned-19 (50 μM) abolished the majority of the NAADP-induced response. **(C).** Average peak Ca^{2+} responses induced by NAADP-AM (1, 10, 100 μM) with and without Ned-19 and Baf-A1 (500 nM). Percentage (from a total of 100–400 cells) of responding (ΔFura-2> 0.02) cells; the number of the responding cells are indicated. **(D).** NAADP (100 nM or 1 μM) failed to induce measurable whole-endolysosomal current in a

NIH-PA Author Manuscript

NIH-PA Author Manuscript

NIH-PA Author Manuscript

vacuole isolated from an INS1 cell; $PI(3,5)P_2$ activated large $I_{TRPML\text{-}L}$ (E_{rev} =3.4 ± 3 mV, n=14; the ratio of current amplitudes at − 30 mV versus −120 mV was ~ 1%) in the same vacuole. (**E).** $PI(3,5)P_2$ activated $I_{TRPML\text{-}L}$ in a vacuole from a *WT* primary pancreatic β-cell. **(F).** *TPC1*$^{-/-}$/*TPC2*$^{-/-}$ primary pancreatic islets exhibit normal concentration-dependent glucose-induced Ca^{2+} responses. Cytosolic [Ca^{2+}] increased significantly in both *WT* and *TPC1*$^{-/-}$/*TPC2*$^{-/-}$ pancreatic islets in response to elevations of the glucose concentration (in mM; 1, 5, 8, 15; G1, G5, G8, and G15) in the perfusion solution (2.5 mM Ca^{2+}). The traces shown are representative of 19 *WT* and 16 *TPC1*$^{-/-}$/*TPC2*$^{-/-}$ islets, respectively. The right panel shows the average peak Ca^{2+} responses induced by 15 mM glucose (G15) in *WT* and *TPC1*$^{-/-}$/*TPC2*$^{-/-}$ pancreatic islets. **(G).** Glucose-induced Ca^{2+} responses in *WT* and *TPC1*$^{-/-}$/*TPC2*$^{-/-}$ pancreatic islets were inhibited by Ned-19 (100 μM). The traces shown are representative of the results obtained in 7 *WT* and 7 *TPC1*$^{-/-}$/*TPC2*$^{-/-}$ islets, respectively. **(H).** NAADP-AM (200 μM) induced bi-phasic Ca^{2+} increases in the presence of 3 mM glucose (Yamasaki et al., 2004) in both *WT* and *TPC1*$^{-/-}$/*TPC2*$^{-/-}$ islets. Traces shown are representative of the results obtained in 2 *WT* and 3 *TPC1*$^{-/-}$/*TPC2*$^{-/-}$ islets, respectively. Data are presented as the mean ± SEM. See also Figure S7.